Int. J. Solids Structures, 1973, Vol. 9, pp. 655 to 670, Pergamon Press. Printed in Great Britain

STRESS-SINGULARITIES DUE TO UNIFORMLY DISTRIBUTED LOADS ALONG STRAIGHT BOUNDARIES

P. S. THEOCARIS†

The National Technical University, Athens (625), Greece

Abstract—The optical method of caustics, as it has been developed for the study of the stress-intensity factors at the crack-tips, was used for the evaluation of the stress-singularities created by uniformly distributed loads applied at a straight boundary in generalized plane-stress problems. The absolute retardations of light rays impinging normally at a plate under conditions of plane stress and partly reflected either on the front, or on the rear face of the plate, are deviated due to the constraint of the plate at the vicinity of the applied load and the refractive index variation. The deviated light rays, when projected on a screen, are concentrated along a singular curve, which is strongly illuminated and forms a *caustic*. It was proved that the shape and size of the caustic depend on the stress singularity at the point of application of the load. Thus, by measuring the dimensions of the caustic, it is possible to evaluate the state of stress at the singularity. The properties of the caustic were studied in relation to the loading mode of the plate.

INTRODUCTION

THE problem of stress distribution in a semi-infinite plate under generalized plane-stress conditions, which is loaded by a concentrated force acting at some point of the straight boundary, which was taken as origin, was solved by Flamant, as early as 1892 [1]. Flamant's solution was based on Boussinesq's three-dimensional solution [2]. While Flamant solved the problem of a concentrated vertical force acting upon the straight boundary, Boussinesq gave in the same year the solution for the case of any inclined force [3].

It has been found by these early solutions that the stress-distribution in the semi-infinite plate is a radial distribution. The polar components of stresses at any point of the plate with polar coordinates r and ϑ are given by the simple relationships:

$$\sigma_r = -\frac{2P}{\pi}\frac{\cos\vartheta}{r}, \qquad \sigma_\vartheta = \tau_{r\vartheta} = 0.$$

Furthermore, it can be readily shown that the radial stress σ_r has the same magnitude at all points of any circle, which is tangent to the straight boundary at the point of contact. If the diameter of the circle is denoted by d, the radial stress component is:

$$\sigma_r = -\frac{2P}{\pi d}.$$

This value holds for all points of the circle except the point of application of load, where a stress singularity appears of the order of r^{-1}.

In order to avoid the existence of stress-singularities at the point of application of loads, Hertz [4] considered the case of two spheres under contact. By defining the circular

† Professor of Theoretical and Applied Mechanics.

or elliptic surface of contact this theory can avoid the stress singularities at the boundary of the surface of contact. The Hertz problem can readily be reduced to the corresponding plane problem for a frictionless cylindrical punch acting upon a semi-infinite space.

If, instead of a concentrated load, a uniformly distributed load along a part of the straight boundary is considered the problem of stress distribution can be solved by superimposing the stresses produced by each of the vertical forces creating the unifor.n distribution. For each of them the components of stresses are obtained by shifting the corresponding curves which express the distribution of each component of stress constructed for a particular place of the concentrated load to new origins defined by the relative position of each concentrated load and the initial one. The complete solution of this problem is given in Timoshenko's classical book [5].

As an application of Hertz's theory Shaw and DeSalvo [6] have recently shown that elasticity plays a significant role in the formation of the plastic zone beneath a flat rigid punch, which differs significantly from the slip-line field assumed initially by Prandtl (who considered the material as plastic-rigid one). They concluded that a blunt indenter yields a plastic-flow zone, corresponding to a slip-line field only if there is a sufficiently small quantity of elastic material beneath the punch, so that the plastic-rigid assumption holds. If the elastic material is sufficiently large, the solution may be based on the elastic Hertz problem, and the elastic–plastic boundary resembles a line of constant maximum elastic shear stress, as it is derived from Hertz's theory.

However, if the applied load is either strictly concentrated or the indenter is not blunt, at the extremities of the contact area of the indenter and the semi-infinite elastic body singularities of the order of r^{-1} appear and these create uncertainties for the stress-field at the vicinity of these areas.

The method of caustics, developed by the author [7], is a unique experimental method suitable for the study of stress-singularities, as well as any other type of stress discontinuities or concentrations due to either a change of the externally applied load, or the geometry of the specimen. According to this method the stress singularity is transformed into an optical singularity expressed by a *caustic* (line of concentration of light-rays), the shape and dimensions of which yield sufficient information for the evaluation of the stress-field at the close vicinity of the singularity. The method was applied up to now to stress singularities created at the tips of single cracks or arrays of cracks [8], as well as to the study of stress-concentrations around small holes drilled at the interior of any two-dimensional stress-field [12].

In this paper the same method is adopted for the study of singularities created by either concentrated loads or uniformly distributed loads, applied at the straight boundary of an elastic half-plane. The experimental evidence, based on the above method on plexiglas plates, corroborated with existing elastic theories concerning the order of singularities for uniformly distributed loads.

THE METHOD OF CAUSTICS

If a monochromatic and coherent light beam, emitted from a He–Ne gas laser, impinges normally on the lateral faces of a thin-plate made of a transparent and optically-isotropic material (such as plexiglas) and subjected to a uniformly distributed load along a part of its straight boundary, it is partially reflected on the front and rear faces of the plate. We are interested in the light rays traversing the plate once, as well as in the light rays reflected

either once on the front, or once on the rear face of the plate. This is because the intensities of these bundles are significant and they readily yield satisfactory caustics [7].

The light rays traversing the plate are retarded along the thickness and, if the principal stress-axes are denoted by 1 and 2, the absolute variations of the optical path along these axes are given by [9]:

$$\Delta s_{t_1} = \Delta s_{t_2} = dc_t(\sigma_1 + \sigma_2). \tag{1}$$

The absolute variations of the optical paths for light-rays reflected on the rear face of the plate are:

$$\Delta s_{r_1} = \Delta s_{r_2} = dc_r(\sigma_1 + \sigma_2) \tag{2}$$

where d is the thickness of the plate, $(\sigma_1 + \sigma_2)$ is the sum of principal stresses c_t is the optical constant of the material for traversing light-rays, and c_r is the optical constant for reflected light-rays at the rear face of the plate.

Interferometric measurements on plexiglas combined with simultaneous measurements of the elastic constants E and ν of the material allowed the evaluation of c_t and c_r from relations:

$$\begin{aligned} c_t &= \frac{1}{E}[(1-2\nu)b - \nu(n-1)] \\ c_r &= \frac{2}{E}[(1-2\nu)b - \nu(n-\tfrac{1}{2})] \end{aligned} \tag{3}$$

where b is Neumann's optical constant of the optically isotropic material and n is the refractive index of the material when unloaded.

The values for the constants of the material were:

$$\begin{gathered} E = 2{\cdot}80 \times 10^4 \text{ Kp/cm}^2 \qquad \nu = 0{\cdot}34 \qquad c_t = -1{\cdot}01 \times 10^{-5} \text{ cm}^2/\text{Kp} \\ c_r = -3{\cdot}24 \times 10^{-5} \text{ cm}^2/\text{Kp}. \end{gathered} \tag{4}$$

The emerging light front $S(x, y, z)$ after traversing the plate, or reflected on the rear face, is deviated and vector $\mathbf{w}$, which expresses the displacement (PP′) of a generic point P on the plate, as it is projected on a reference plane at distance z_r from the mid-plane of the plate (Fig. 1), is given by:

$$\mathbf{w}_{t,r} = -z_r \operatorname{grad} \Delta s_{t,r}(x, y). \tag{5}$$

Introducing either relation (1) or (2) for the transmitted or the reflected light rays we obtain:

$$\mathbf{w} = C \operatorname{grad}(\sigma_1 + \sigma_2) \tag{6}$$

where constant C takes the values:

and

$$\begin{aligned} C &= C_t = -z_r dc_t \qquad \text{(for transmitted light)} \\ C &= C_r = -z_r dc_r \qquad \text{(for reflected light on the rear face).} \end{aligned} \tag{7}$$

Similarly, it can be shown that the deviation **w** of the reflected light-rays on the front face are given by:

$$\mathbf{w}_f = -z_r \frac{vd}{E} \operatorname{grad}(\sigma_1 + \sigma_2)$$

which may be also expressed by relation (6) if one puts:

$$C = C_f = -z_r \frac{vd}{E}. \tag{8}$$

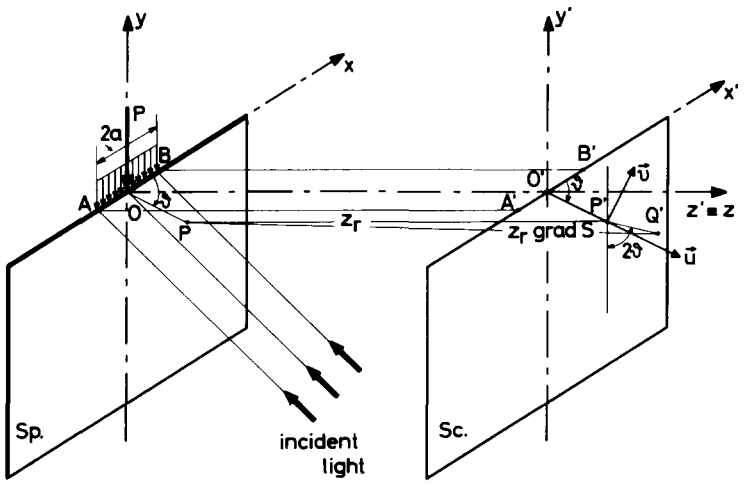

FIG. 1. Geometry of semi-infinite plate partly loaded along its straight boundary and relative position of specimen and reference screen.

UNIFORMLY DISTRIBUTED LOAD ALONG A PART OF THE STRAIGHT BOUNDARY

Consider a plate of an elastic, homogeneous and isotropic material in a generalized plane-stress condition occupying the negative half-plane and a reference frame $0xy$, as indicated in Fig. 2. The plate is uniformly loaded along the part AB = 2a of the straight boundaries by a normal stress σ. A generic point P of the plate at distances r, r_1 and r_2 from points O, A and B respectively, and angles subtended by r, r_1 and r_2 and the positive x-axis equal to ϑ, ϑ_1 and ϑ_2 respectively, is in a state of stress, defined by the function $\Phi(z)$ of the complex variable $z = (x+iy)$ given by [10]:

$$\Phi(z) = \frac{1}{2\pi i} \int_{-a}^{+a} \frac{\sigma}{(t-z)} dt = \frac{\sigma}{2\pi i} \ln \frac{(z-a)}{(z+a)}. \tag{9}$$

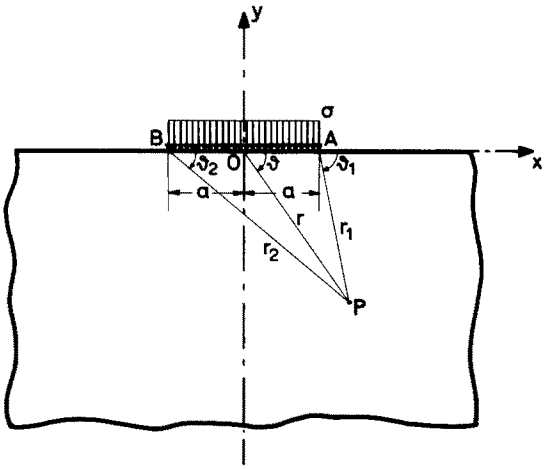

FIG. 2. Geometry of semi-infinite plate uniformly loaded along a part of its straight boundary and the related reference frame.

Differentiating $\Phi(z)$ with respect to z we obtain:

$$\frac{d\Phi}{dz} = \frac{\sigma a}{\pi i(z^2 - a^2)} \tag{10}$$

$$\overline{\frac{d\Phi}{dz}} = \frac{\sigma a}{\pi i(a^2 - \overline{z^2})} \tag{11}$$

$$\frac{d^2\Phi}{dz^2} = \frac{2\sigma a z}{\pi i(z^2 - a^2)^2} \tag{12}$$

where $\overline{\Phi'(z)}$ is the complex conjugate of $\Phi'(z)$.

Since it is valid that $z = r e^{-i\vartheta}$, $z_1 = r_1 e^{-i\vartheta_1}$ and $z_2 = r_2 e^{-i\vartheta_2}$, while $z_1 = (z-a)$ and $z_2 = (z+a)$, relations (9) to (12) may be written as:

$$\Phi(z) = \frac{\sigma}{2\pi}\left[-i \ln \frac{r_1}{r_2} + (\vartheta_2 - \vartheta_1)\right] \tag{13}$$

$$\frac{d\Phi}{dz} = \frac{\sigma a}{\pi i r_1 r_2} e^{i(\vartheta_1 + \vartheta_2)} \tag{14}$$

$$\overline{\frac{d\Phi}{dz}} = -\frac{\sigma a}{\pi i r_1 r_2} e^{-i(\vartheta_1 + \vartheta_2)} \tag{15}$$

and

$$\frac{d^2\Phi}{dz^2} = \frac{2i\sigma a r}{\pi r_1^2 r_2^2} e^{i[2(\vartheta_1 + \vartheta_2) - \vartheta]}. \tag{16}$$

The biaxial state of stress at any point of the plate under load is expressed in complex form by:

$$4Re\Phi(z) = (\sigma_1 + \sigma_2) \tag{17}$$

where the function $\Phi(z) = [u(x, y) + iv(x, y)]$ is expressed by equations (9) or (13). Introducing relation (17) into equation (6) and taking into consideration the Cauchy–Riemann relationships, we obtain for w in complex form that:

$$w = C\left(\frac{\partial u}{\partial x} + \mathrm{i}\frac{\partial u}{\partial y}\right)$$

where w is referred to a reference frame with origin the projection P′ of every point P of the plate on the reference plane Sc (Fig. 1). If w is referred to a fixed reference frame $0'x'y'$, it becomes:

$$W = (x' + iy') \tag{18}$$

with

$$x' = \left(x + C\frac{\partial u}{\partial x}\right) \quad \text{and} \quad y' = \left(y + C\frac{\partial u}{\partial y}\right). \tag{19}$$

Quantity W expresses the projections on screen Sc of the deviations of the reflected or transmitted light-rays. These rays at the constrained zone, surrounding the singularities of the stress-field, due to a significant lateral contraction there, as well as a considerable variation of the refractive index, are deviated by different amounts, depending on the slope of lateral faces and the variation of the refractive index. These rays are concentrated at an envelope, because of the singularity, which is strongly illuminated and forms a *caustic*. This envelope represents a singular curve for W. The conditions for existence of a singularity is the zeroing of the Jacobian determinant $J = \partial(x', y')/\partial(r, \vartheta) = 0$. This relation, after some algebra, yields:

$$4C\left[\frac{\mathrm{d}^2\Phi}{\mathrm{d}z^2}\right] = 1. \tag{20}$$

Relation (20) expresses the equation of the initial curve creating the caustic. The envelope of this curve is given by the set of equations (20) and (18), which may be written as:

$$\left.\begin{aligned} 4C\left[\frac{\mathrm{d}^2\Phi}{\mathrm{d}z^2}\right] &= 1 \\ W &= z - 4C\overline{\frac{\mathrm{d}\Phi(z)}{\mathrm{d}z}} \end{aligned}\right\}. \tag{21}$$

Introducing equations (10) or (13) into relations (20) and (21) we obtain for the equation of the initial curve that:

$$\frac{8C\sigma}{\pi a^2}\left|\frac{a^3 z}{(a^2 - z^2)^2}\right| = 1. \tag{22}$$

The above relations hold for a parallel light beam impinging on the plate. If the light-rays are divergent (or convergent), the magnification ratio λ_i is defined by:

$$\lambda_i = \frac{z_r + z_i}{z_i}$$

where z_i is the distance between the focus of light beam and the mid-plane of the specimen, while z_r is the distance between the mid-plane and the reference plane Sc. This ratio must

be introduced into relation (22), which becomes:

$$\frac{8C\sigma}{\pi a^2 \lambda_i}\left|\frac{a^3 z}{(a^2-z^2)^2}\right| = 1.$$

In order to simplify the above expressions we put:

$$C^* = \frac{8C\sigma}{\pi a^2 \lambda_i} \tag{23}$$

and introduce normalized coordinates to the semi-width a of the uniformly applied load σ, so that:

$$z_0 = z/a, \qquad r_0 = r/a, \qquad r_{01} = r_1/a, \qquad r_{02} = r_2/a, \qquad w_0 = w/a. \tag{24}$$

Then, the expression for the initial curve becomes:

$$C^*\left|\frac{z_0}{(1-z_0^2)^2}\right| = 1 \tag{25}$$

which, after some rearrangement, yields:

$$r_0^4 - 2r_0^2 \cos 2\vartheta - C^* r_0 + 1 = 0. \tag{26}$$

Equation (26) yields the expression of the initial curve in polar coordinates r_0 and ϑ. From relation (26) it can be derived that:

$$\cos 2\vartheta = (r_0^4 - C^* r_0 + 1)/(2r_0^2) \tag{27}$$

where angle ϑ for the type of loading considered here is varying between $0 \geq \vartheta \geq -\pi$.

For a generic value of r_0 there is a corresponding value for ϑ, if it is valid that:

$$|r_0^4 - C^* r_0 + 1| \leq 2r_0^2. \tag{28}$$

In this case the value for $\cos 2\vartheta$ is fixed, which yields two values for the angle 2ϑ, that is $2\vartheta_1$ and $2\vartheta_2$ in the interval $-2\pi \leq 2\vartheta_1, 2\vartheta_2 \leq 0$. The angles ϑ_1 and ϑ_2 are connected by the relation $(\vartheta_1 + \vartheta_2) = -\pi$. Thus, $\vartheta_2 = -(\pi + \vartheta_1)$. This relation indicates that the singular curves expressed by relation (26) are symmetric with respect to the $0x$-axis ($\vartheta = \pm\pi/2$). This result was expected from the symmetry of the problem.

The equation for the epicycloid created by the initial curve of equation (26) is given by:

$$W = \lambda_i[z - (4C^*/\lambda_i)\overline{\mathrm{d}\Phi}/\mathrm{d}z] = \lambda_i\left[z + \frac{4C^*}{\lambda_i}\frac{\sigma a}{\pi i(\bar{z}^2 - a^2)}\right]$$

which, when it is referred to the normalized coordinates, expressed by relations (24), and if relation (25) is taken into account, yields:

$$W_0 = \lambda_i[r_0 e^{-i\vartheta} - i(r_0^2 e^{-2i\vartheta} - 1)/2r_0]. \tag{29}$$

This relation readily yields the parametric equations of the epicycloid:

$$\begin{aligned} X_0 &= \lambda_i[r_0 \cos\vartheta - (r_0^2 \sin 2\vartheta)/2r_0] \\ Y_0 &= \lambda_i[-r_0 \sin\vartheta - (r_0^2 \cos 2\vartheta - 1)/2r_0] \end{aligned} \tag{30}$$

or

$$\left.\begin{aligned} X_0 &= \lambda_i r_0[\cos\vartheta - \sin 2\vartheta/2] \\ Y_0 &= -\lambda_i r_0\left[\sin\vartheta + \frac{1}{2}\left(\cos 2\vartheta - \frac{1}{r_0^2}\right)\right] \end{aligned}\right\}. \tag{31}$$

In these relations r_0 and ϑ are related by the equation of the initial curve (26).

DISCUSSION OF PARTICULAR CASES

(i) *Concentrated load* ($a = 0$)

Consider first the case when $C^* \to \infty$, that is when $a \to 0$. In this case the initial curve becomes a half-circle with radius r_0 given by:

$$r_0 = (C^*)^{\frac{1}{3}}. \tag{32}$$

Indeed, equation (26) becomes:

$$(C^*)^{\frac{4}{3}} - 2(C^*)^{\frac{2}{3}}\cos 2\vartheta - (C^*)^{\frac{2}{3}} + 1 = 0.$$

Since for $C^* \to \infty$ the second and fourth terms are insignificant, the above equation is satisfied identically. The parametric equations of the epicycloid become:

$$\left.\begin{aligned} X_0 &= \lambda_i(C^*)^{\frac{1}{3}}[\cos\vartheta - \sin 2\vartheta/2] \\ Y_0 &= -\lambda_i(C^*)^{\frac{1}{3}}[\sin\vartheta + \tfrac{1}{2}\{\cos 2\vartheta - (C^*)^{-\frac{2}{3}}\}] \end{aligned}\right\}. \tag{33}$$

(ii) *Uniform load extended to infinity* ($C^* \to 0$)

If $C^* \to 0$, then it may be taken that $a \to \infty$. Equation (25) of the initial curve may also be written as:

$$r_{01}^2 \cdot r_{02}^2 = C^* r_0. \tag{34}$$

We consider first point B for which we have $r_{01} \simeq 2$ and $r_0 \simeq 1$. From equation (34) it can be deduced that $r_{02} = \frac{1}{2}(C^*)^{\frac{1}{2}}$. Similarly, for point A we have $r_{01} = \frac{1}{2}(C^*)^{\frac{1}{2}}$. For $C^* \to 0$ we have as initial curves half-circumferences of a very small radius at the extremities A and B of the loaded boundary $x = \pm a$ and $y = 0$. The corresponding epicycloids are expressed by:

$$W = \lambda_i\left[z + \frac{4C}{\lambda_i}\frac{\sigma a}{\pi i r_1 r_2}e^{-i(\vartheta_1+\vartheta_2)}\right]. \tag{35}$$

By putting into equation (35) $r_1 = 2a$, $\vartheta_1 = -\pi$ and $z = (-a + r_2 e^{-i\vartheta_2})$ we obtain, after some straightforward calculations, that:

$$W_{02} = \lambda_i e^{-i\vartheta_2}\left[r_{02} + \frac{iC^*}{4r_{02}}\right] \tag{36}$$

where $W_{02} = (W_{01} + 1)$. But, we have already found for this case that $r_{02} = \frac{1}{2}(C^*)^{\frac{1}{2}}$, then:

$$W_{02} = \frac{\lambda_i}{2}(C^*)^{\frac{1}{2}} e^{-i\vartheta_2}[1 + i] \tag{37}$$

which yields:

$$X_{02} = \frac{\lambda_i}{2}(C^*)^{\frac{1}{2}}(\cos\vartheta_2 + \sin\vartheta_2)$$
$$Y_{02} = \frac{\lambda_i}{2}(C^*)^{\frac{1}{2}}(\cos\vartheta_2 - \sin\vartheta_2) \tag{38}$$

Similarly, for the other extremity of the loaded boundary A we have:

$$X_{01} = \frac{\lambda_i}{2}(C^*)^{\frac{1}{2}}[\cos\vartheta_1 - \sin\vartheta_1]$$
$$Y_{01} = \frac{\lambda_i}{2}(C^*)^{\frac{1}{2}}[\cos\vartheta_1 + \sin\vartheta_1] \tag{39}$$

and

$$W_{01} = \frac{\lambda_i}{2}(C^*)^{\frac{1}{2}}\, e^{-i\vartheta_1}[1-i]. \tag{40}$$

(iii) *General case for* $a \neq (0, \infty)$

In the general case the width of the applied load $2a$ is significant and it does not tend to infinity. Then, from relation (27) we obtain:

$$\vartheta_1 = -\tfrac{1}{2}\cos^{-1}\left(\frac{r_0^4 - C^* r_0 + 1}{2r_0^2}\right)$$
$$\vartheta_2 = \tfrac{1}{2}\cos^{-1}\left(\frac{r_0^4 - C^* r_0 + 1}{2r_0^2}\right) - \pi. \tag{41}$$

For each value of the radius r satisfying the inequality (28) we define two values for angle ϑ from equations (41), and therefore two points of the initial curve, which yield afterwards, by applying relation (29), the corresponding points on the epicycloid.

However, this procedure by a series of trials with arbitrary values for r_0 is rather cumbersome, and it does not yield a full picture of the shape of the epicycloid. It is better practice to select various angles for ϑ and define the corresponding values for the polar radii r_1 and r_2. In this case it is necessary to solve the equation of the fourth order:

$$r_0^4 - 2r_0^2\cos 2\vartheta - C^* r_0 + 1 = 0. \tag{42}$$

Since equation (42) does not contain a third-degree term, and since the coefficient $(-C^*)$ of the first-degree term is always negative, this equation has solutions $r_{01,2,3,4}$ given by:

$$r_{01} = \tfrac{1}{2}[(s_1)^{\frac{1}{2}} + (s_2)^{\frac{1}{2}} + (s_3)^{\frac{1}{2}}]$$
$$r_{02} = \tfrac{1}{2}[(s_1)^{\frac{1}{2}} - (s_2)^{\frac{1}{2}} - (s_3)^{\frac{1}{2}}]$$
$$r_{03} = \tfrac{1}{2}[-(s_1)^{\frac{1}{2}} + (s_2)^{\frac{1}{2}} - (s_3)^{\frac{1}{2}}]$$
$$r_{04} = \tfrac{1}{2}[-(s_1)^{\frac{1}{2}} - (s_2)^{\frac{1}{2}} + (s_3)^{\frac{1}{2}}] \tag{43}$$

where $s_{1,2,3}$ are the roots of the corresponding resolvent equation of the third degree expressed by:

$$s^3 - 4\cos 2\vartheta s^2 - 4\sin^2 2\vartheta s - (C^*)^2 = 0. \tag{44}$$

Since it is always $-(C^*)^2 < 0$ and $-4\sin^2 2\vartheta < 0$, the third-degree equation (44) can have either one positive and two negative roots, or one positive and two complex roots, when the fourth-order equation must have respectively either four complex roots or two real and two complex roots. Therefore, since we seek real roots for the initial equation (42), we are interested for the solution of its resolvent equation yielding one real and two complex roots. In order to find this solution we form the equation of the third-degree:

$$y^3 + py + q = 0 \tag{45}$$

with

$$p = -\tfrac{4}{3}(3 + \cos^2 2\vartheta) \tag{46}$$

and

$$q = -\tfrac{1}{27}[27(C^*)^2 + 144\cos 2\vartheta - 16\cos^3 2\vartheta] \tag{47}$$

which has a real root:

$$y_1 = (\mathrm{A} + \mathrm{B}) \tag{48}$$

and two complex roots:

$$y_{2,3} = -\frac{(\mathrm{A}+\mathrm{B})}{2} \pm \mathrm{i}\sqrt{3}\frac{\mathrm{A}-\mathrm{B}}{2} \tag{49}$$

where

$$\mathrm{A} = \left[-\frac{q}{2} + \left(\frac{q^2}{4} + \frac{p^3}{27}\right)^{\frac{1}{2}}\right]^{\frac{1}{3}} \tag{50}$$

$$\mathrm{B} = \left[-\frac{q}{2} - \left(\frac{q^2}{4} + \frac{p^3}{27}\right)^{\frac{1}{2}}\right]^{\frac{1}{3}}. \tag{51}$$

In order that equation (45) must have one real and two complex roots it is necessary that:

$$q^2/4 + p^3/27 \geq 0. \tag{52}$$

The roots s_1, s_2, s_3 of the initial resolvent equation (equation 44) are given by:

$$s_{1,2,3} = (y_{1,2,3} + \tfrac{4}{3}\cos 2\vartheta). \tag{53}$$

Introducing the values for $s_{1,2,3}$ into equation (43) we define easily the roots $r_{01,2,3,4}$ of the initial fourth order equation. From these roots two are real and positive, if $(q^2/4 + p^3/27) > 0$, and they coincide to only one, if $(q^2/4 + p^3/27) = 0$. It can be readily found that the two positive roots for equation (42) are expressed by:

$$r_{01,2} = \tfrac{1}{2}[\{\mathrm{A} + \mathrm{B} + \tfrac{4}{3}\cos 2\vartheta\}^{\frac{1}{2}} \pm \{-(\mathrm{A}+\mathrm{B}) + \tfrac{8}{3}\cos 2\vartheta + [\{-(\mathrm{A}+\mathrm{B}) + \tfrac{8}{3}\cos 2\vartheta\}^2 + 3(\mathrm{A}-\mathrm{B})^2]^{\frac{1}{2}}\}^{\frac{1}{2}}]. \tag{54}$$

Equation (54) shows that the initial curve passes always by two points of each polar radius r_0.

In order to define if the initial curve is either a continuous curve or it possesses two branches, symmetric with respect to the y-axis, we examine the case for which $\vartheta = \pi/2$.

For $\vartheta = \pi/2$ it is valid that $\cos 2\vartheta = -1$, $p = -\frac{16}{3}$, $q = [-(C^*)^2 + \frac{128}{27}]$ and therefore the expression:

$$\frac{q^2}{4} + \frac{p^3}{27} \geq 0$$

yields:

$$C^* \geq \frac{16\sqrt{3}}{9}. \tag{55}$$

If the sign of equality is taken in equation (55) the values for $q, A, B, y_{1,2,3}$ and $s_{1,2,3}$ become:

$$q = -2(\tfrac{4}{3})^3, \qquad A = B = \tfrac{4}{3}$$

$$y_1 = \tfrac{8}{3} \quad \text{and} \quad y_2 = y_3 = -\tfrac{4}{3}$$

$$s_1 = \tfrac{4}{3} \quad \text{and} \quad s_2 = s_3 = -\tfrac{8}{3}.$$

In the case when $s_2 = s_3 =$ negative, instead of equations (43), we have the simplified relations: $r_{01} = r_{02} = \frac{1}{2}[(s_1)^{\frac{1}{2}}]$ and the roots of the fourth-order equation take the values:

$$r_{01} = r_{02} = \frac{1}{\sqrt{3}}. \tag{56}$$

Thus, for $C^* > (16\sqrt{3})/9$ we have two branches of the initial curve, one of them enveloping the other. For $C^* < (16\sqrt{3})/9$ there are two separate branches of the initial curve enveloping either extremity of the loading area (points A and B in Fig. 2). For $C^* = (16\sqrt{3})/9$ the two distinct branches are tangent along the y-axis ($\vartheta = \pi/2$) at the point $r = 1/\sqrt{3}$.

NUMERICAL AND EXPERIMENTAL APPLICATIONS

For the study of the development of the constrained zones at the vicinity of the uniformly applied load, a series of computations were undertaken in the IBM 1620 computer of the Technical University, where the solution of the equation (42) was programmed and the shapes of the initial curves and the corresponding generalized epicycloids were directly plotted for various configurations of applied loads and optical set-ups.

The governing parameter for the type of the epicycloid is the global constant C^*, which contains the characteristics of the load (magnitude of uniform applied stress σ, and area of application of the load σ), as well as the characteristics of the specimen (thickness d and optical constants $c_{t,r,f}$) and the optical set-up (distance z_r and magnification ratio λ_i). The computer programmes were prepared for C^* varying between $C^* = 1000$ and $C^* = 1$. The case $C^* = 1000$ for the usual optical arrangement utilized in the experiments corresponded to the case of concentrated load. As the values for C^* were diminishing, either the loading width $2a$ was increasing, or the applied stress was decreasing.

Figure 3 shows the cases for concentrated load (Fig. 3a) where $C^* \to \infty$ and $C^* = 3{\cdot}34$ (Fig. 3b), while Fig. 4 shows the cases for $C^* = 3$ and $C^* = 1$ respectively. The cases presented in Fig. 4 correspond to values of $C^* < (16\sqrt{3})/9$ and therefore the initial curves in these cases contain two separate branches (curves with open circles).

It is clearly shown in these plots that the two branches of the epicycloids form a shape of crescent for the case of concentrated load. However, for $C^* \to \infty$ there are also parts of the epicycloids at $x = 0$ and $y = \pm\infty$.

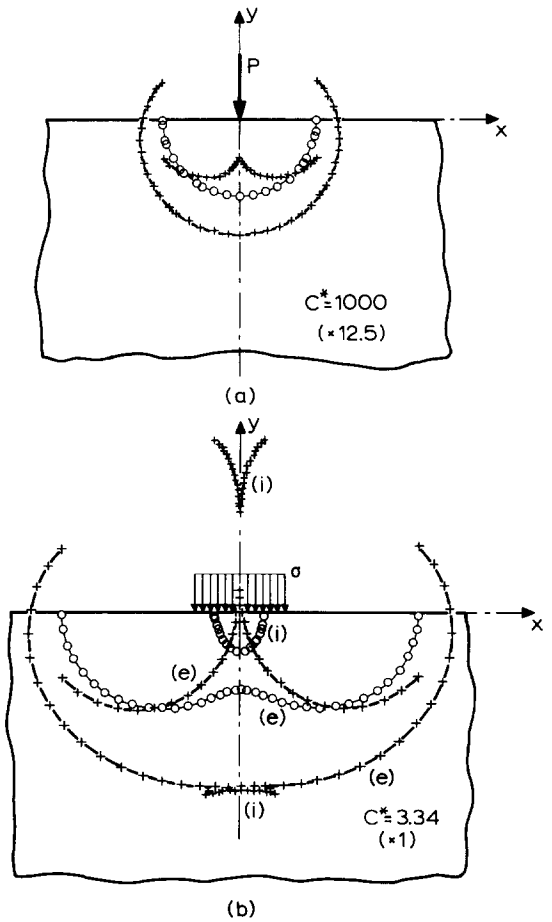

FIG. 3. Computer plots for the initial curve and the corresponding generalized epicycloid for cases where $C^* > C^*_{cr}$ ($C^*_{cr} = (16\sqrt{3})/9$). Figure 3a corresponds to the case of concentrated load ($C^* = 1000$) and Fig. 3b to the case where $C^* = 3{\cdot}34$.

As the values for C^* are decreasing the internal boundary of the crescent is angularly displaced toward the center of the loading area and the parts of the epicycloid at infinity are now displaced, approaching the two main branches, (Fig. 3b, parts (e)) at the vicinity of the y-axis (parts (i)). Furthermore, the initial curve, which for $C^* \to \infty$ was a circle and a point at the origin, it contains now two branches, the internal one surrounding the origin and yielding the parts (i) of the epicycloid, and the external part like a half-eight, which corresponds to the main branches of epicycloid (parts (e)).

For values of C^* below the critical value $C^*_{cr} = (16\sqrt{3})/9$ the parts (e) and (i) of the initial curve are divided symmetrically and joined together, forming two continuous curves, symmetric with respect to the y-axis (parts (l) and (r) in Fig. 4). Similarly, the branches (i) and (e) of the epicycloid are divided along the y-axis and the internal (i) and (e) branches are joined together (parts (l) and (r) respectively). For the case $C^* = 3$ shown in Fig. 4a the internal branches of the epicycloid (l) and (r) are tangents along the y-axis.

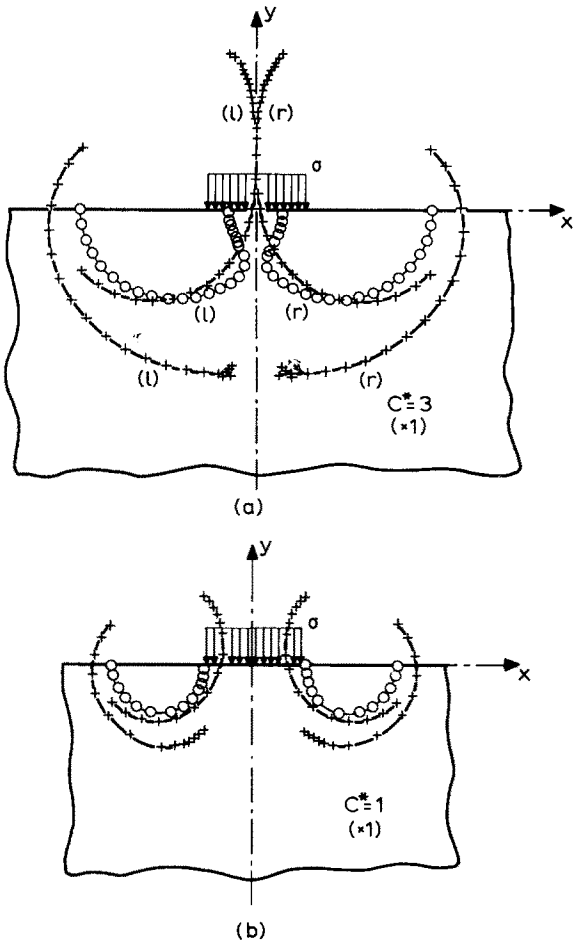

FIG. 4. Computer plots for the initial curve and the corresponding generalized epicycloid for cases where $C^* < C_{cr}$. Figure 4a corresponds to case where $C^* = 3{\cdot}0$, while 4b shows the case where $C^* = 1{\cdot}0$.

For smaller values of C^* ($C^* = 1$) the left and right branches of the initial curve and the epicycloids are totally separated and they again resemble to circular arcs, as for the other extreme case, where $C^* \to \infty$.

In order to check the theory with experimental results, a series of tests were undertaken with thin orthogonal plexiglas plates subjected to compression at a part of their larger straight boundary. The thickness of the plate was of the order of 3 mm and their width and height were sufficient to simulate a half-space. The plate was supported to a specially designed zig, suitable to avoid any buckling of the thin plate when compressed, without introducing secondary loadings, other than the compression applied by the flat indenter. The load was applied through a symmetric wedge made of plexiglas of variable width. This load was kept always symmetric to the vertical axis of the plate. The dimensions of the wedge were properly selected to create a uniform stress distribution at the surface of contact between plate and wedge.

The plexiglas plates were conveniently selected with almost flat surfaces, which were optically tested to yield sparse interferograms when unloaded. The plates were interposed in a monochromatic light beam emitted from a He–Ne gas laser. The light beam was widened through a lens and reflected on both lateral surfaces of the plate. The distance z_r between the mid-surface of the plate and the reference screen Sc (Fig. 1) varied between $z_r = 120$ cm and $z_r = 160$ cm. A photographic camera recorded the interference pattern with the caustics which was projected on the reference screen Sc. The magnification ratio varied between $\lambda_i = 6{\cdot}7$ and $\lambda_i = 9{\cdot}5$.

Figure 5 presents parts of the interferograms at the vicinity of the loading area of the plate together with the caustics formed by reflections on the front and rear faces of the plate. Figure 5a corresponds to the case of a concentrated load, while Fig. 5b corresponds to the case where $C^* > C^*_{cr} = (16\sqrt{3})/9$. The shapes of epicycloids for $C^* < C^*_{cr}$ are shown in Fig. 6. While Fig. 6a shows the case corresponding to the plot of Fig. 4a, Fig. 6b, with separated parts of epicycloids, presents the case for a large length of application of load and it is related to the plot of Fig. 4b.

The differences in the relative positions of the epicycloids obtained experimentally and shown in Figs. 5 and 6 and the corresponding computer plots in Figs. 3 and 4 are mainly due to the fact that while in the computer-plots the global constants C^*, incorporating the optical constant of the material (c) were taken the same for reflections on front and rear faces of the plate, in the experiments the values of constants c_r and c_f for reflections on the rear and the front faces respectively are different [11]. The values of these constants for plexiglas were measured interferometrically and found to be:

$$c_r = -3{\cdot}24 \times 10^{-5}\ \text{cm}^2/\text{Kp} \qquad c_f = 1{\cdot}21 \times 10^{-5}\ \text{cm}^2/\text{Kp}.$$

This explains the difference in relative positions between the external and internal branches of the epicycloids found experimentally.

Another possible source of eventual discrepancies between theoretical plots and experimental epicycloids is the impossibility of creating a uniformly distributed state of stress at the contact area between plate and loading wedge. Although the shape, dimensions and the material used for the wedge were carefully selected, and the two contact surfaces were checked to be flat and well polished, it was expected in the experiments that some discrepancies in the uniformity of constant stresses must exist.

However, if one introduces the suitable values for the optical constants c_r and c_f for the two branches of the epicycloid, the experimentally formed curves coincide well with the theoretical ones.

CONCLUSIONS

A potential and simple experimental method was developed for the study of the type of stress-singularities created at the loaded boundary in semi-infinite plates submitted to a uniformly distributed load along a part of the straight boundary. The method was based on principles of geometric optics and the stress singularity was transformed into an optical singularity under the form of a *caustic* (line of concentration of light-rays). The form and dimensions of the optical singularity yielded the type of the existing stress singularity at the vicinity of the applied load, as well as the amount of externally applied load, since the shape of the generalized epicycloid yields the value for the radius of its initial curve and this,

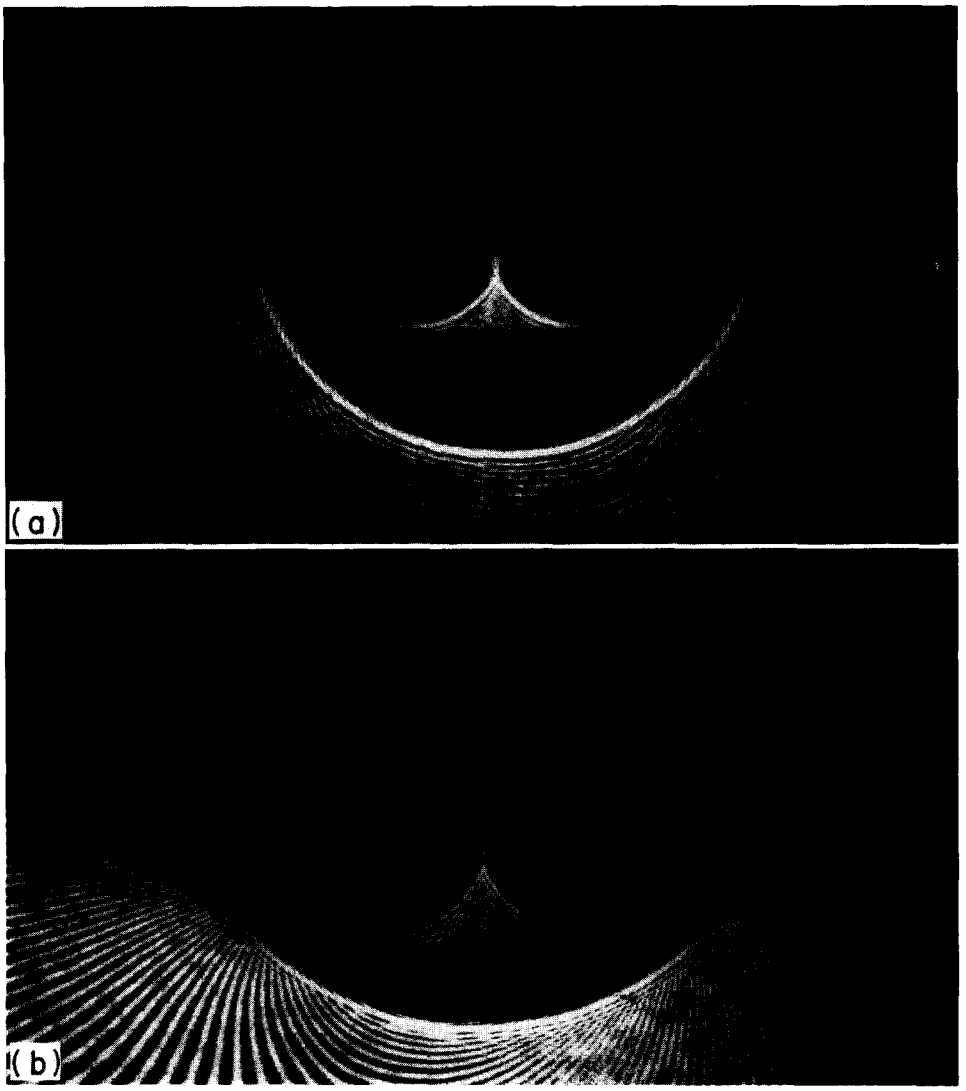

FIG. 5. Caustics of generalized epicycloids experimentally obtained for concentrated load ($C^* \to \infty$) (a) and for $C^* > C^*_{cr}$ (b).

[*facing* p. 668

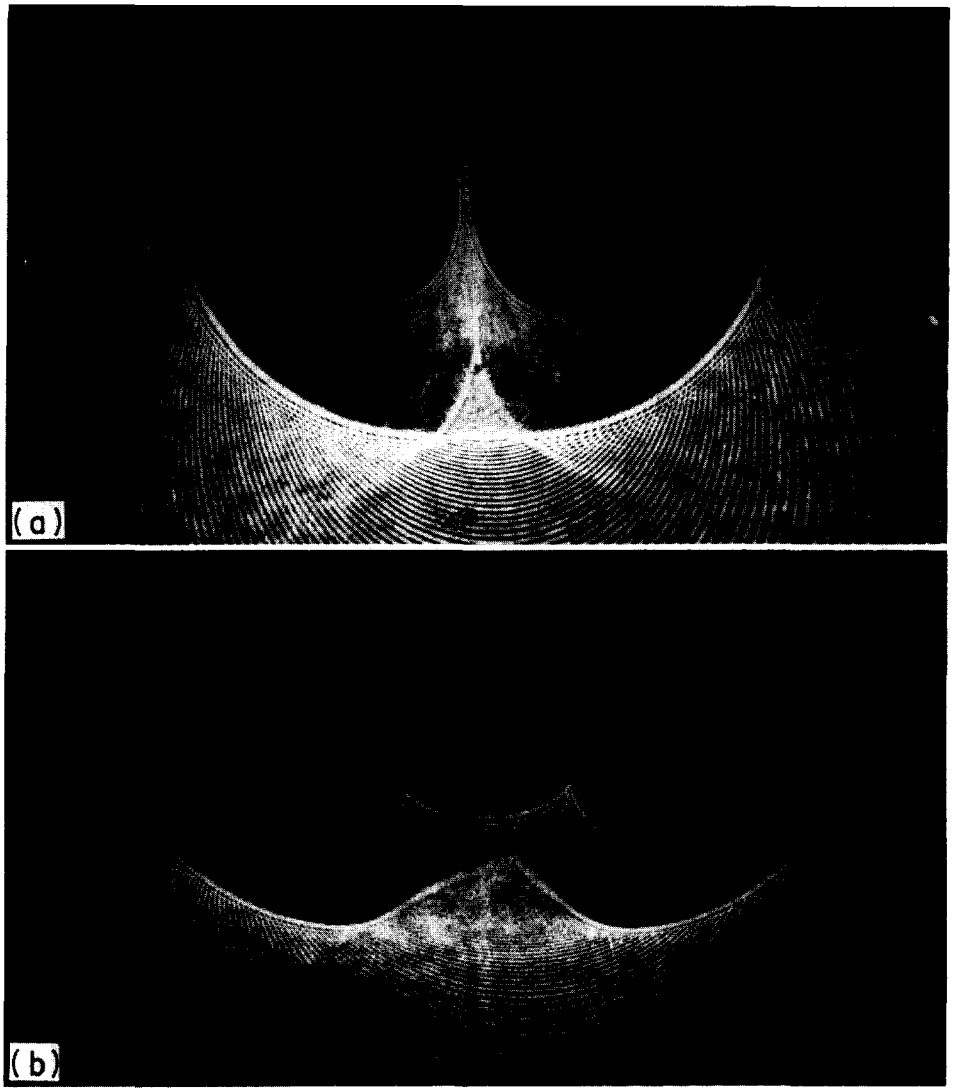

FIG. 6. Caustics of generalized epicycloids experimentally obtained for two cases where $C^* < C^*_{cr}$.

in turn, allows the evaluation of constant C^* and therefore the stress σ (from either of equations (7) or (8) and equation (23)).

It was shown that the order of singularity given by theory for the case of concentrated or uniformly distributed loads along a straight boundary is in agreement with the experimental results found by the caustics.

Furthermore, since the externally applied load or uniform stress can be readily measured during the experiments, the same relationships allow the measurement of variation of the optical constants at the highly constrained areas at the vicinity of the loaded boundary. Indeed, if the material is either viscoelastic or elastic–plastic, it is expected at the highly constrained zone that an enclave will be created, which is either strongly viscoelastic or fully plastic, and in this zone the characteristic mechanical and optical properties of the perfectly elastic material cease to be valid.

The method yields a powerful means for studying the variation of these properties of the material in the highly-constrained zone, by following the development of the shape and the geometry of the caustic, created at the vicinity of the singularity.

The method was used with success for the study of singularities created at the tips of cracks [6–8], as well as for the study of stress concentrations in two-dimensional stress fields created by the existence of holes [12].

REFERENCES

[1] A. FLAMANT, De l'influence sur la flexion des poutres de la position superficielle de la charge, *Annales des Ponts et Chaussées* **VI**, 228–242 (1893); see also: A. FLAMANT; Sur la repartition des pressions dans un solide rectangulaire chargé transversalement. *Comptes Rendus Acad. Sci.* **114**, 1465 (1892).

[2] J. BOUSSINESQ, *Application des potentiels à l'étude de l'équilibre et du mouvement des solides élastiques*, Gauthier–Villars (1885).

[3] J. BOUSSINESQ, Perturbations locales que produit audessous d'elle une forte charge repartie uniformement l'ong d'une droite normale aux débords à la surface supérieure d'une poutre rectangulaire et de longueur indefinie posée de champ soit sur un sol horizontal, soit sur deux appuis traversaux equidistants de la charge. *Comptes Rendus Acad. Sci.* **114**, 1510 (1892).

[4] H. HERTZ, *Gesammelte Werke* **1**, 155 (1895); see also H. HERTZ; Über die Berechnung fester elastischer Körper, 174–196 (1881).

[5] S. TIMOSHENKO, *Theory of Elasticity*, McGraw-Hill, pp. 82–93 (1934).

[6] M. C. SHAW and G. J. DESALVO, A New Approach to Plasticity and its Application to Blunt Two-Dimensional Intenters, *Trans. ASME* **92**, Ser. B, 469 (1970).

[7] P. S. THEOCARIS, Local Yielding Around a Crack-Tip in Plexiglas, *J. appl. Mech.*, **37**, *Trans. ASME*; **92**, Ser. E, 409 (1970).

[8] P. S. THEOCARIS, The Reflected Shadow Method for the Study of Constrained Zones in Cracked Plates, *Applied Optics* **10**, 2240 (1971); see also: P. S. THEOCARIS, Constrained Zones in a Periodic Array of Collinear Equal Cracks, *Int. J. Mech. Sci.* **14**, 79 (1972); see also: P. S. THEOCARIS, A Theoretical Consideration of the Constrained Zones in an Array of Interacting Collinear and Asymmetric Cracks, *Acta Mech.* **15**, 239 (1973).

[9] H. FAVRE, Sur une nouvelle méthode d'optique de détermination des tensions intérieures, *Revue d'Optique théorique et instrumentale* **8**, 5 (1929).

[10] N. I. MUSKHELISHVILI, *Some Basic Problems of Mathematical Theory of Elasticity*, pp. 373. P. Noordhoff (1953).

[11] P. S. THEOCARIS, Complex Stress Intensity Factors at Bifurcated Cracks, *J. Mech. Phys. Solids* **20**, 287 (1972); see also: P. S. THEOCARIS and C. BLONZOU, Symmetric Branching of Cracks in Plexiglas, *Materialprüfung* **15**, 215 (1973).

[12] P. S. THEOCARIS, The Optical Stress-Rosette Based on Caustics, *Applied Optics* **12**, 185 (1973).

(*Received* 9 *August* 1972)

Абстракт—Используется оптический метод каустик, разработанный для исследования факторов интенсивности напряжений в конце трещины, с целью определения сингулярностей в напряжениях, созданных вследствие приложения постоянно распределенных нагрузок к прямой границе, в обобщенных задачах плоского напряженного состояния. Абсолютные запаздывания лучей света, падающих нормально к пластинке в условиях плоского напряжения, и частью отраженных как на лицевой так и на нижней стороне пластинки, отклоняются благодаря ограничению свободы пластинки в окрестности приложенной нагрузки и вследствие изменения показателя степени преломления. Во время проекции на экран, сосредоточиваются отклоненные лучи света вдоль особой кривой, которая сильно освещена и принимает форму *каустики*. Доказано что форма и размер каустики зависят от особенности напряжений, в точке приложения нагрузки. Таким образом, путем измерения размеров каустики, можно определить напряженное состояние в сингулярной точке. Исследуются свойства каустики в зависимости от характера нагрузки пластинки.